Carbohydrate Polymers 102 (2014) 400–408

Contents lists available at ScienceDirect

Carbohydrate Polymers

journal homepage: www.elsevier.com/locate/carbpol

Supercritical fluid assisted production of chitosan oligomers micrometric powders

Zhe Du, Yu-Bin Shen, Chuan Tang, Yi-Xin Guan*, Shan-Jing Yao, Zi-Qiang Zhu

Department of Chemical and Biological Engineering, Zhejiang University, Hangzhou 310027, China

ARTICLE INFO

Article history:
Received 8 August 2013
Received in revised form
19 November 2013
Accepted 21 November 2013
Available online 1 December 2013

Keywords:
Supercritical fluid assisted atomization
Hydrodynamic cavitation mixer
Chitosan oligomers
Micronization

ABSTRACT

Chitosan oligomers (O-chitosan) micrometric particles were produced from aqueous solution using a novel process, i.e. supercritical fluid assisted atomization introduced by hydrodynamic cavitation mixer (SAA-HCM). Hydrodynamic cavitation was introduced to enhance mass transfer and facilitate the mixing between SC-CO_2 and liquid solution for fine particles formation. Well defined, separated and spherical microparticles were obtained, and the particles size could be well controlled with narrow distribution ranging from 0.5 μm to 3 μm. XRD patterns showed amorphous structure of O-chitosan microparticles. FTIR, TGA and DSC analyses confirmed that no change in molecular structure and thermal stability after SAA-HCM processing, while the water content was between 5.8% and 8.4%. Finally, tap densities were determined to be below 0.45 g/cm^3 indicating hollow or porous structures of microparticles. By tuning process parameters, theoretical mass median aerodynamic sizes lied inside respirable range of 1–2 μm, which presented the potential of the O-chitosan microparticles in application as inhaled dry powders. SAA-HCM was demonstrated to be very useful in particle size engineering.

1. Introduction

Powder systems composed of microparticles are of great interest in drug formulations where they serve directly as delivery systems or as building blocks of innovative drug products. Microparticulate dosage offers several advantages over conventional drug delivery methods, such as high efficacy and extended administration flexibility (Reverchon & Antonacci, 2006). Depending on the application, powder products should be tailor-made with respect to size distribution and morphology (Buttini, Colombo, Rossi, Sonvico, & Colombo, 2012). For example, the aerodynamic size of powders to be used for dry inhalation therapies should range between 1 and 5 μm (Amidi, Mastrobattista, Jiskoot, & Hennink, 2010). Supercritical fluid (SCF) based micronization processes had been developed with characteristics like mild operation temperature and minimum organic solvent residues and were successfully applied to polymer processing (Knez, Markočič, Novak, & Hrnčič, 2011). Unfortunately, there are still some difficulties in producing microparticles of hydrophilic biopolymers like chitosan or its oligomers (O-chitosan) using SCF based techniques including RESS, PGSS and SAS. On the one hand, these biopolymers have nearly no solubility in SC-CO_2; and on the other hand, SC-CO_2 has hardly any antisolvent effect on their aqueous solutions.

Supercritical fluid assisted atomization (SAA) was proposed by Reverchon (2002), which makes use of the atomization assisting effect of SC-CO_2 to obtain fine particles. This technique has been investigated for micronization of various kinds of polymers, either water soluble or insoluble (Reverchon & Antonacci, 2006, 2007b). The original SAA process has been then improved adding the possibility to work in the precipitator at reduced pressures to work with highly thermolabile compounds (Adami, Liparoti, Izzo, Pappalardo, & Reverchon, 2012; Adami, Liparoti, & Reverchon, 2011; Liparoti, Adami, & Reverchon, 2012). In 2008, our group (Cai, Guan, Yao, & Zhu, 2008) established an improved SAA process and introduced the hydrodynamic cavitation phenomenon to intensify the mixing between SC-CO_2 and solution (SAA-HCM). In SAA-HCM process, an orifice plate is used as the mixing point and the hydrodynamic cavitation generator. The emerging and collapse of CO_2 transient cavities results in convective and enhanced mixing, and a "homogeneous dispersion" is finally formed in the mixer with moderate residence time, which is preferable for preventing polymer from thermal degradation (Wang, Guan, Yao, & Zhu, 2010). So far SAA-HCM process has been successfully employed in micronization of diverse substances with good morphology and size control (Du, Guan, Yao, & Zhu, 2011; Du, Tang, Guan, Yao, & Zhu, 2013; Miao, Yu, Du, Guan, Yao, & Zhu, 2010; Wang, Guan, Yao, & Zhu, 2011). The capability of SAA-HCM to process aqueous solution makes this process promising for chitosan and O-chitosan micronization. Meanwhile, the expansion of CO_2 in the precipitator would reduce water vapor pressure and the inert atmosphere could also prevent oligosaccharides from being oxidized.

* Corresponding author. Tel.: +86 571 87951982; fax: +86 571 87951982.
E-mail address: guanyx@zju.edu.cn (Y.-X. Guan).

0144-8617/$ – see front matter © 2013 Elsevier Ltd. All rights reserved.
http://dx.doi.org/10.1016/j.carbpol.2013.11.029

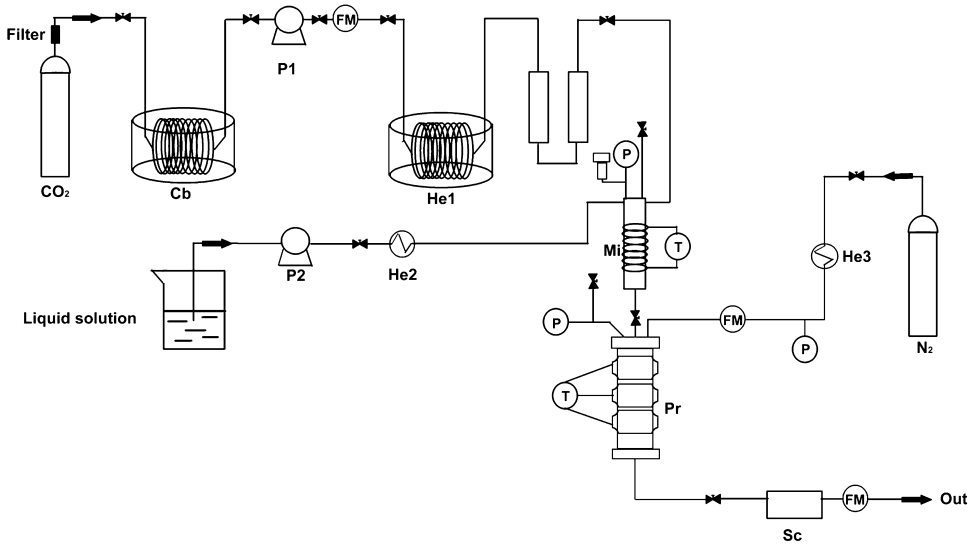

Fig. 1. Schematic diagram of the supercritical fluid assisted atomization introduced by hydrodynamic cavitation mixer (SAA-HCM) process (Cb, cooling bath; He1, He2 and He3, heat exchanger; P1 and P2, high pressure pumps; FM, mass flow meter; Mi, mixer; Pr, precipitator; Sc, solvent condenser).

Till now, several studies have been successfully carried out using SAA process to produce chitosan microparticles (Adami & Reverchon, 2012; Reverchon & Adami, 2013; Reverchon & Antonacci, 2006, 2007a). However, these studies all used acidic solutions for chitosan micronization and the concentration range was limited due to the viscosity increase of polymer. Moreover, no O-chitosan was processed. It is well known that O-chitosan has higher water solubility and lower viscosity than chitosan itself, accompanied by enhanced hygroscopicity and susceptibility to processing conditions (Muzzarelli, 2010; Muzzarelli, Stanic, & Ramos, 1999). O-chitosan supplied to wounded human tissues exerts key biochemical effects leading to healing (Muzzarelli, 2009). The aim of this study is to verify the feasibility of SAA-HCM process for O-chitosan micronization using water as solvent. The effects of processing conditions on product properties were elucidated and the influences of the treatment on polymer structure integrity were analyzed to investigate the ability of this process in O-chitosan particle engineering without damaging the molecular structure. The density and theoretical aerodynamic properties was also evaluated to further demonstrate the potential of O-chitosan microparticles in pharmaceutical application.

2. Materials and methods

2.1. Materials

Chitosan oligomers (O-chitosan) with a degree of deacetylation of 91.3% and mass mean molecular weight of 1000 Da were purchased from Qingdao Yunzhou Biochemistry Co. Ltd. (Qingdao, China), and the main components are chitosan pentamer and hexamer. Carbon dioxide (CO_2, purity of 99%) and nitrogen (N_2, purity of 99%) was supplied by Hangzhou Jingong Gas Co. Ltd. (Hangzhou, China). Deionized water was prepared in our laboratory. All other chemicals used were of analytical grade.

2.2. Experimental apparatus

As illustrated in Fig. 1, the SAA-HCM apparatus is characterized by three feed lines, i.e. supercritical CO_2, the solution and the drying gas N_2, respectively, as well as three vessels: the mixer, the precipitator, and the condenser. Liquid CO_2 from a high pressure pump (P1) was heated in a heating bath (He1) to achieve the desired temperature and then sent into the mixer (Mi). Liquid solution was fed by a high pressure pump (P2), after heated (He2) and also delivered into the mixer where SC-CO_2 contacted with the solution. The mixture was sprayed through a thin-wall stainless steel nozzle (i.d. 200 μm) located in the precipitator (Pr) to generate atomization. The precipitator was operated at 0.13 MPa, and a controlled flow of 20 N dm^3/min of N_2 heated by a heat exchanger (He3) was sent into the precipitator to assist the evaporation of solvent. The dried particles were collected by a stainless steel filter with a 0.5 μm pore size at the bottom of the precipitator. The mixture of CO_2, N_2 and solvent vapor then passed through a cooling unit (Sc) to condense the solvent. Detailed description of the layout and operating procedures of this process is presented elsewhere (Cai, Guan, Yao, & Zhu, 2008).

2.3. Particles size and distribution

Samples of O-chitosan microparticles produced were observed by scanning electron microscope (SEM) (Sirion, FEI, Netherlands) to analyze their morphology. For particle size distribution (PSD) calculation, SEM images were conducted with particle image analysis software (Nano Measurer 1.2.5, Fudan University, China). At least 2000 target particles were considered in each PSD calculation performed. The statistical results were fitted by Systat Software (TableCurve 2D 5.01, Systat Software Inc., USA) to give size distribution curves.

2.4. Particles solid state characterizations

A Fourier transform infrared spectrometer (Nicolet 5700, ThermoNicolet, USA) was used to analyze structural stability of O-chitosan after SAA-HCM processing. O-chitosan samples were mixed with anhydrous KBr and compressed into a film with an evacuable die. The films were placed into the nitrogen-purged sample chamber and spectra were recorded. 256 scans between 400 and 4000 cm^{-1} with resolution of 4 cm^{-1} were co-added.

Thermal behavior of O-chitosan samples was analyzed by differential scanning calorimeter (Q200, TA Instruments, USA) and thermogravimetric analyzer (Pyris 1, Perkin Elmer, USA), respectively. For DSC, samples of unprocessed O-chitosan and

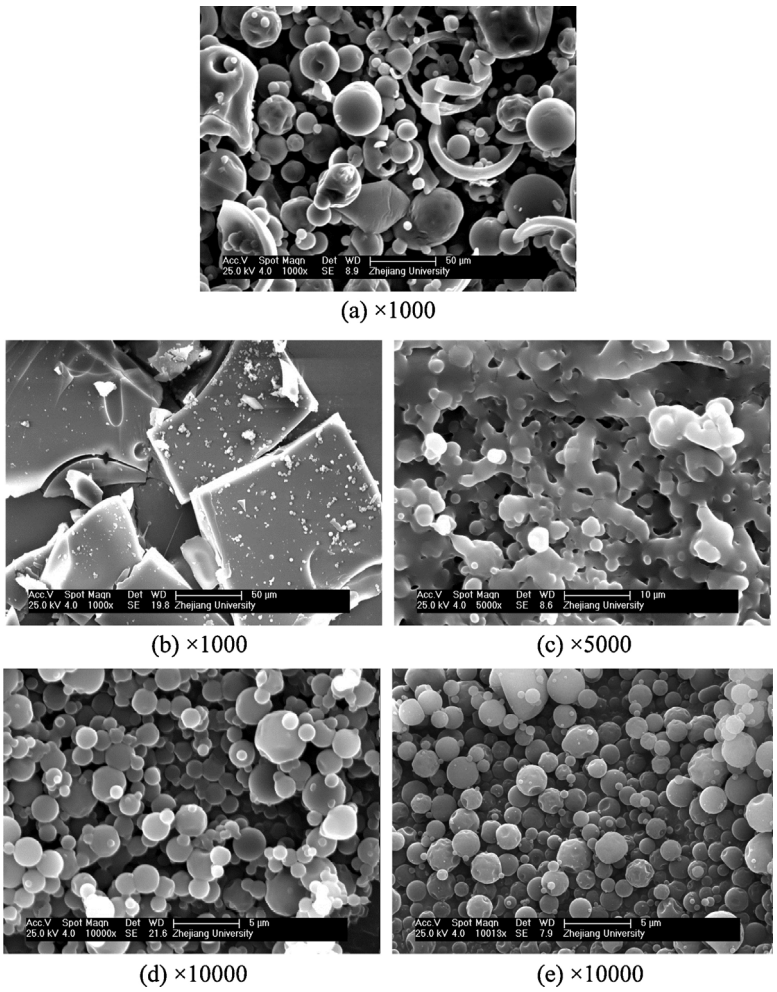

Fig. 2. O-chitosan raw material and microparticles produced at different precipitator temperature by SAA-HCM: (a) raw material; (b) 65 °C; (c) 75 °C; (d) 90 °C; and (e) 120 °C.

microparticles (4–6 mg) were sealed in aluminum pans with vented lids and loaded in sample cells under nitrogen, and then scanned from 25 to 120 °C at 10 °C/min. For TGA, samples of unprocessed O-chitosan and microparticles (3–13 mg) were loaded on open platinum TGA pans suspended from a microbalance and heated from 25 to 550 °C at 10 °C/min.

Diffraction patterns of unprocessed O-chitosan and precipitated powders were obtained using an X-ray diffractometer (X'Pert PRD, PANalytical, The Netherlands). The generator voltage was 40 kV and the tube current was 40 mA with Ni-filtered Cu $K\alpha$ radiation. 2θ ranged between 5° and 80° with a scan rate of 10 s/step and a step size of 0.0167°.

2.5. Particles tap density

The tap density of the O-chitosan dry powder was estimated using a microtap test approach (Bailey, Gorman, Munson, & Berkland, 2008). Briefly, dry powder samples were added to glass tubes previously weighed. The tubes were weighed again to determine the mass of powder and tapped 100 times to compress the powder. To approximate the volume of the powder, another identical pre-weighed glass tube was filled with water in parallel to the same level of the powder. Assuming a density of 1 g/cm^3 for water, the volume could be determined by weighing the tube containing the water. The powder density was then calculated by dividing the mass of powder by the volume of water. Based upon the tap density, the theoretical mass median aerodynamic diameter (*MMADt*) of the particles could be estimated as follows:

$$MMADt = MMD\sqrt{\left(\frac{\rho}{\rho_0}\right)\chi}$$

where *MMD* is the mass median geometric diameter, which equals to volume median geometric diameter (*VMD*) assuming particles of different sizes have the same density (Amidi, Pellikaan, de Boer, Crommelin, Hennink, & Jiskoot, 2008); ρ is the particle density which can be approximated by tap density (Vanbever, Mintzes, Wang, Nice, Chen, Batycky, Langer, & Edwards, 1999); ρ_0 is the reference density and equals to 1 g/cm^3; χ is the shape factor which equals to 1 for spherical particles.

3. Results and discussion

Since the solubility of CO_2 in water is quite limited (Wiebe, 1941), the operating points of the solution–CO_2 mixture would always drop into the two-phase region when using water as solvent. Therefore the mixing of SC-CO_2 with the solution is one of the key factors to determine the efficiency of the process. Considering the improved SAA process, a "homogeneous dispersion" in the HCM was formed due to the convective and enhanced mixing. While flowing through the nozzle, CO_2 firstly expands to

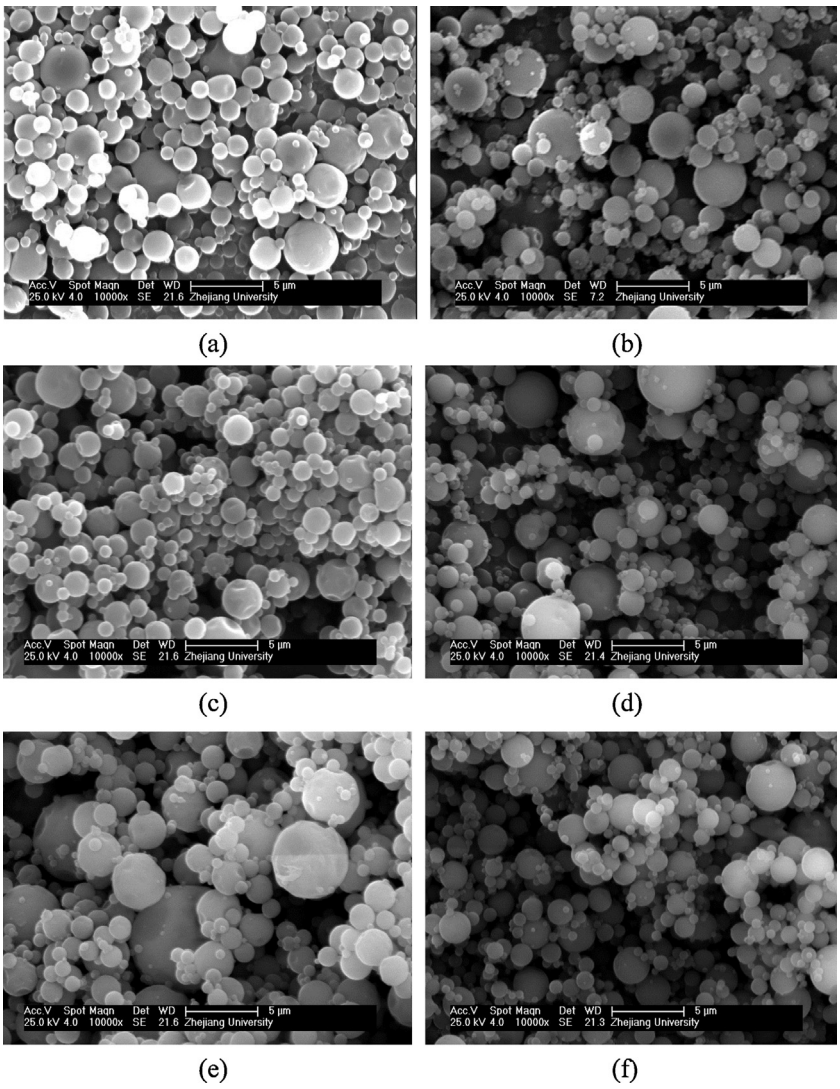

Fig. 3. O-chitosan microparticles produced at different process parameters by SAA-HCM: (a) run 3; (b) run 5; (c) run 8; (d) run 10; (e) run 14; and (f) run 15.

reduce the flow area of the liquid, causing an enhanced pneumatic atomization and producing primary droplets. Then decompressive atomization breaks up the primary droplets, due to the subsequent explosion of dissolved CO_2 from them, into smaller secondary ones, which are dried into microparticles according to the "one droplet one particle" mechanism (Reverchon & Antonacci, 2006).

3.1. Particle engineering by SAA-HCM

The operation conditions of SAA-HCM process include temperature (*MT*) and pressure (*P*) in the mixer and mass flow ratio (*R*) which determine the operating points based on the phase equilibrium of the CO_2–water–solute ternary system, the precipitator temperature (*PT*) which is related to evaporation efficiency and thermal stress exerted on the substance, and the solute concentration (*C*), which should be regarded as an important factor for particle morphologies and the size distributions. In this work, the effects of process parameters on particle morphology and size were studied in detail, and the feasibility of micronizaiton operation using acidic aqueous solutions (hydrochloric/acetic acid) was also discussed. All of the operating parameters are summarized in Table 1.

3.1.1. Influence of precipitator temperature

The O-chitosan raw material consists of large particles or shells with size ranging from several to hundreds of microns, as shown in Fig. 2(a). In the precipitator, the drying of atomization-induced droplets forms the microparticles according to the "one droplet one particle" mechanism. As a rule, the precipitator temperature (*PT*) determines the efficiency of solvent evaporation. Starting the experimental at relatively low *PTs* of 65 °C and 75 °C, no separated particles were obtained, as shown in Fig. 2(b) and (c). Coalescence among particles was common for the sample produced at *PT* of 75 °C, and lower *PT* of 65 °C further deteriorated and induced agglomeration of particles into films. The reason is that the low *PTs* did not offer efficient water evaporation and recondensation of moisture could happen on the particles collected on the filter. As a contrast, only coalescent particles were obtained at similar precipitator temperature range for hydrophilic biopolymers like cellulose derivatives (Wang, Guan, Yao, & Zhu, 2010), while the higher hygroscopicity of O-chitosan gave rise to the films formed at *PT* of 65 °C. When *PT* increased to 90 °C, separated and well-defined spherical dried particles were collected, as shown in Fig. 2(d). Further increase of *PT* also ensured successful production of separated microparticles but with a few deflated patterns as shown in Fig. 2(e). The appearance of particle deflation was due to the fast evaporation of water that

Table 1
SAA-HCM process parameters of experiments performed on O-chitosan.

Run no.	*PT* (°C)	*MT* (°C)	*P* (MPa)	*R* (CO_2/solution)	*C* (g/L)
Effect of precipitator temperature					
1	65	70	9.5	1.8	10
2	75	70	9.5	1.8	10
3	90	70	9.5	1.8	10
4	120	70	9.5	1.8	10
Effect of mixer temperature					
5	90	50	9.5	1.8	10
3	90	70	9.5	1.8	10
6	90	90	9.5	1.8	10
Effect of mixer pressure					
7	90	70	8.5	1.8	10
3	90	70	9.5	1.8	10
8	90	70	11.5	1.8	10
9	90	70	13.5	1.8	10
Effect of mass flow ratio (CO_2/solution)					
3	90	70	9.5	1.8	10
10	90	70	9.5	1.5	10
11	90	70	9.5	1.2	10
Effect of solution concentration					
12	90	70	9.5	1.8	3
13	90	70	9.5	1.8	5
3	90	70	9.5	1.8	10
14	90	70	9.5	1.8	30
Processablility on acidic solutions					
15[a]	90	70	9.5	1.8	10
16[b]	90	70	9.5	1.8	10

PT, precipitator temperature; *MT*, mixer temperature; *P*, mixer pressure; *C*, solution concentration; *R*, mass flow ratio of CO_2/solution.
[a] 0.01 M HCl.
[b] 1% (v/v) HAc.

increased the instability of the droplets, which were also affected by the vapor bubble formation inside them at temperature higher than solvent boiling point (Wang, Guan, Yao, & Zhu, 2011). Combining the efficient solvent evaporation and preserved particle uniformity, 90 °C should be appropriate for the O-chitosan/water system.

3.1.2. Influence of temperature and pressure in the mixer

According to the high-pressure vapor–liquid equilibrium (VLE) of the selected ternary CO_2/water/O-chitosan system, the temperature and pressure in the mixer (*MT* and *P*) determine the composition of the two-phase flow through the mixer and the nozzle and therefore affect the atomization effect. As shown in Fig. 3(a)–(c), microparticles produced at different *MTs* and *Ps* all represented morphology of separated, well-defined spheres. Qualitative evaluation can be made to the images to recognize that most of the particles were in the range of 0.5–5 μm. Generally, *MT* had a weak influence on particle sizes, the mean diameters of O-chitosan microparticles only changed a little around 1.20 μm while changing *MT* and the size distribution curves mainly overlapped. As shown in Fig. 4(a), the particle size became smaller and the particle size distribution became narrower toward smaller sizes with the increase of *P*. When *P* was set at 8.5 MPa, the largest diameter corresponding to 90% (X_{90}) of the total particle volume was 3.7 μm and particles smaller than 1 μm only occupied less than 10% of the total particle volume.

The effect of *MT* on particle size was taken into account in two aspects. On the one hand, the CO_2 solubility in the solution decreased as *MT* increased, thus the effect of dissolved CO_2 on the pneumatic and decompressive atomization weakened. On the other hand, the increase of *MT* directly reduced the viscosity and the surface tension of the solution, which was favorable for enhanced atomization. These two aspects counteracted and

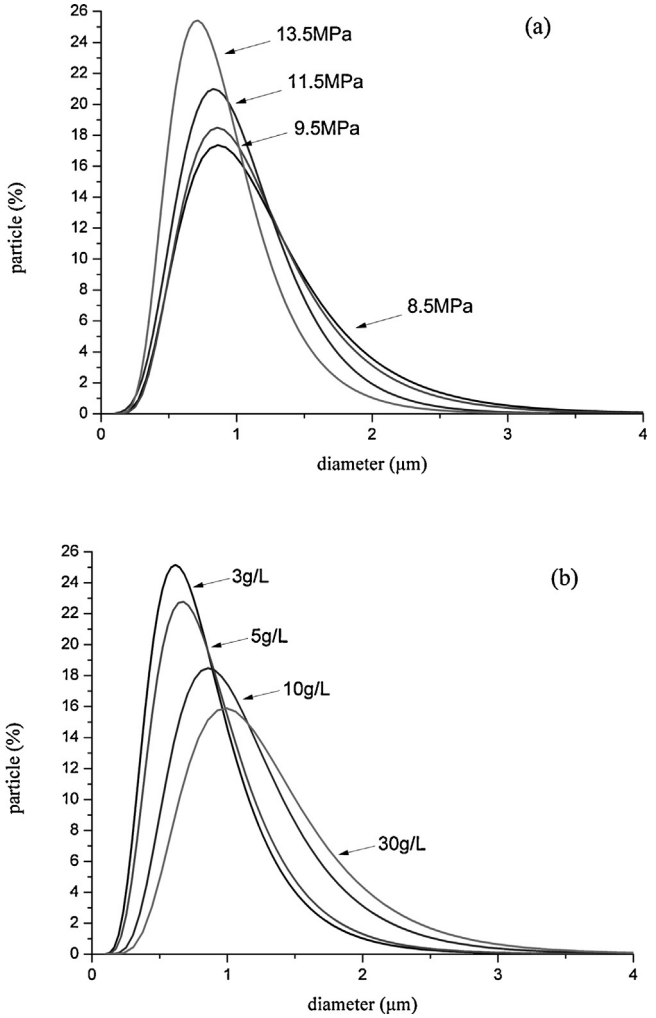

Fig. 4. Particle size distributions of O-chitosan microparticles by SAA-HCM in terms of particle number: (a) effect of pressures and (b) effect of solution concentrations.

could be comparable, leading to the similar particle sizes and overlapped size distributions. As for the effect of *P* on particles size, the increase of *P* elevated the pressure drop through the nozzle, inputting higher energy during liquid breakup. Meanwhile, the CO_2 content in the solution increased with *P*, leading to the reduction of viscosity and surface tension of the solution and subsequently more drastic atomization to form both smaller primary and secondary droplets. Therefore, smaller particles were obtained with narrower size distributions.

3.1.3. Influence of mass flow ratio

Changing the mass flow ratio between CO_2 and solution (*R*) did not give rise to observable differences in particle morphology, as seen in Fig. 3(a) and (d). However, with the decreasing *R*, particle sizes became larger and size distributions became broader. Unlike organic solvent systems, the miscibility between CO_2 and water was quite limited and the operating point always dropped into the vapor/liquid coexistence region. Therefore the influence of *R* on CO_2 content in the solution was negligible. Nevertheless, the increase of *R* reduced the flow area of the solution, which was squeezed into thinner ligaments and subsequently smaller droplets (Caputo, Adami, & Reverchon, 2010). At last, smaller particles were collected. In summary, crucial consideration should be laid on selecting *R* to ensure the efficiency of SAA-HCM. Too low flow ratio can induce chock in the nozzle and sometimes

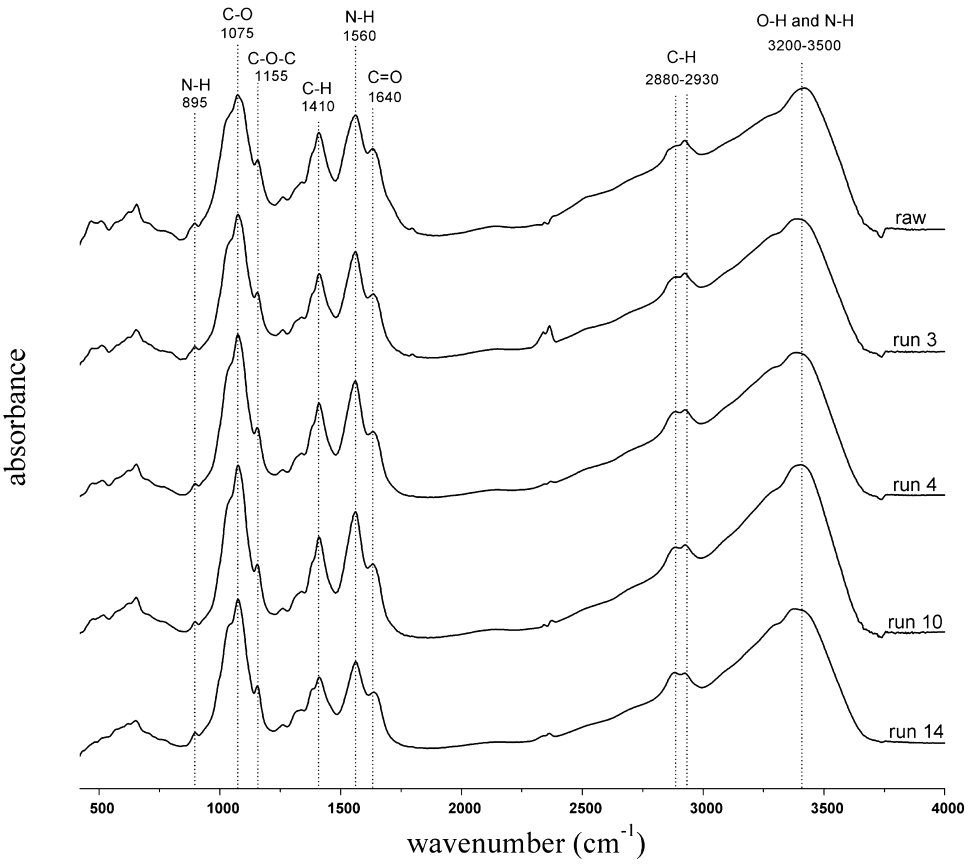

Fig. 5. FTIR spectra of O-chitosan raw material and SAA-HCM processed O-chitosan microparticles.

insufficient energy supply in the precipitator, while too high flow ratio would lead to low productivity. In the case of O-chitosan/water system, flow ratios lower than 1.0 usually caused problems of lack of evaporation or absorption of moisture on the collected product. Normally, *R* ranging from 1.2 to 2.0 would be suitable.

3.1.4. Influence of solution concentration

Unlike micronization with highly viscous chitosan solutions (Reverchon & Antonacci, 2006), SAA-HCM process can be successfully operated on a wide range of O-chitosan solution concentrations without causing viscosity overrun. However, too high of O-chitosan concentration might bring evaporation deficiencies due to the elevated vapor pressure. In the range of 3–30 g/L in this work, well defined, separated and spherical microparticles could always be obtained, as shown in Fig. 3(a) and (e) for partial results. The influence of solution concentration on particle size can be seen in Fig. 4(b). As concentration increased, the particles became larger and the PSD became broader. While operating with dilute solution (3 g/L), particles with sizes smaller than 0.5 μm were present which can be useful for injection purposes (Adami, Osseo, & Reverchon, 2009). Increasing O-chitosan concentration to 10 g/L led to microparticles with more than 80% of volume in the size range of 1–3 μm which may find potential in inhalation. At concentration of 30 g/L, the X_{90} was as large as 4.9 μm and particles smaller than 1 μm only occupied less than 5% of the total particle volume.

In fact, the solution concentration could notably influence the atomization process by affecting the viscosity and the surface tension of the solution. When operating at higher concentrations, the elevated viscosity and surface tension weakened the atomization, which induced larger droplets and subsequently larger particles with broader size distributions.

3.1.5. Processability with acidic aqueous solutions

To investigate the feasibility of SAA-HCM process on O-chitosan acidic solutions, sets of experiments on hydrochloric acid and acetic acid aqueous solution were carried out, using 0.01 M HCl and 1% (v/v) HAc, respectively. The acidification did not induce observable changes on particle morphology and well separated particles were always produced, as evident in Fig. 3(f) for a typical result. The feasibility of SAA-HCM to produce O-chitosan microparticles from acidic aqueous solutions makes the co-precipitation of composite O-chitosan/protein particles possible, specifically for insulin which was also successfully processed using dilute acidic aqueous solutions (Du, Tang, Guan, Yao, & Zhu, 2013).

3.2. Particles solid state characterization

3.2.1. Structural analysis

Fig. 5 gives the FTIR spectra of O-chitosan raw material and SAA-HCM produced O-chitosan microparticles. The characteristic peaks of O-chitosan (Kiechel & Schauer, 2013; Kim, Lee, Lee, & Park, 2003; Kumar & Koh, 2013; Prasertsung, Damrongsakkul, Terashima, Saito, & Takai, 2012) can be assigned as follows: the broad band in the region of 3200–3500 cm^{-1} resulting from the overlapping absorption of O—H and N—H stretching, two smaller bands between 2880 and 2930 cm^{-1} arising from C—H stretching, one band at 1640 cm^{-1} from C=O stretching of amide I, one band at 1560 cm^{-1} from N—H bending in primary and secondary amine in amide II, one band at 1410 cm^{-1} due to the asymmetric stretching of C—H in CH_2, two bands at 1155 cm^{-1} and 1075 cm^{-1} from bridge C—O—C stretching in glycosidic linkage between O-chitosan monomers and C—O stretching, respectively, and one band at 895 cm^{-1} due to N—H wagging. These main absorption bands of O-chitosan microparticles all remained identical compared with raw material, demonstrating

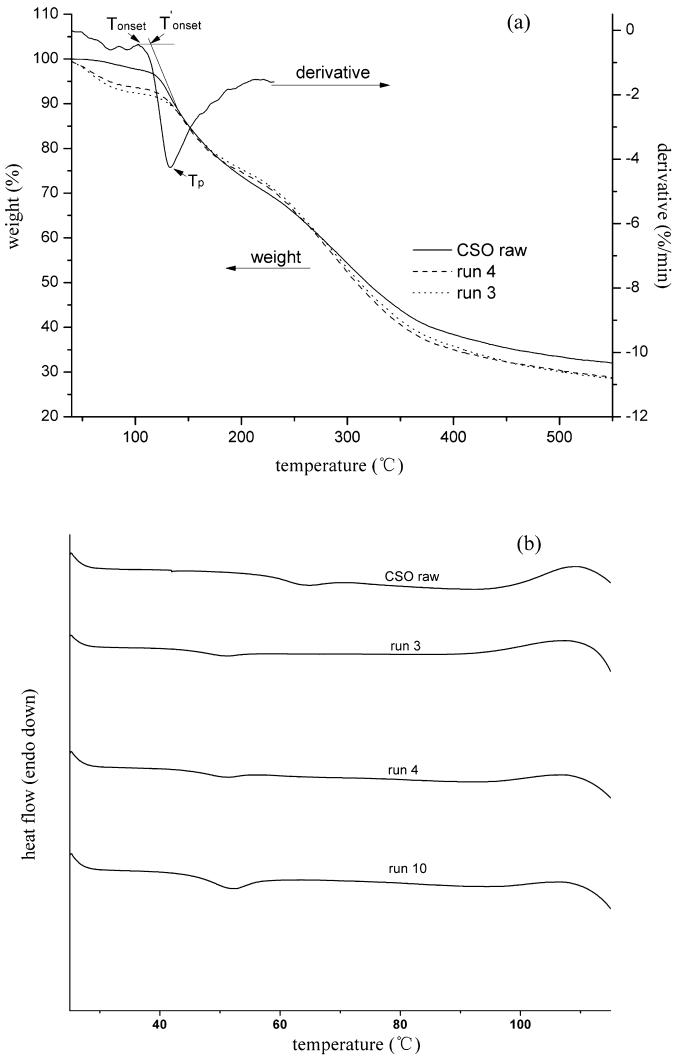

Fig. 6. Thermograms of O-chitosan raw material and SAA-HCM processed O-chitosan microparticles: (a) TGA and (b) DSC.

that no significant change occurred in O-chitosan structure during SAA-HCM processing.

Diffraction patterns from XRD analysis revealed that the raw material had very low crystallinity, and the SAA-HCM produced microparticles were completely amorphous (data not shown). The fast drying in the precipitator did not allow O-chitosan molecules to crystallize into ordered structure. Low crystallinity may imply faster dissolution of O-chitosan microparticles in body fluids and favorable for drug delivery.

3.2.2. Thermal analyses

The TGA and DSC thermograms of O-chitosan raw material and SAA-HCM produced O-chitosan microparticles are shown in Fig. 6. According to the TGA curves in Fig. 6(a), the first stage of weight loss over the temperature range of 40–90 °C was attributed to the evaporation of adsorbed water (Zeng, Qin, Chi, Wang, Ku, & Li, 2007), which also caused the broad endotherm in the same temperature range in DSC thermograms, as seen in Fig. 6(b). It has been widely recognized that polysaccharides usually have strong affinity for water and can be readily hydrated. In O-chitosan molecules, the water molecules are associated with hydrophilic amine groups and hydroxyl groups. As presented in Table 2, the water contents obtained from the first stage of TGA thermograms for O-chitosan microparticles were significantly higher than that of commercial raw material, which was only 2.40 ± 0.11%. As discussed previously, amorphous structure of O-chitosan microparticles was induced, while the O-chitosan raw material showed slight crystallinity. Herein the less ordered structure of SAA-HCM processed O-chitosan might have contributed to the higher water content (Kittur, Prashanth, Sankar, & Tharanathan, 2002). However, the dissolving and dehydration process itself seemed to be the main reason for water content difference, because the water contents of the O-chitosan microparticles differed greatly depending on the operating parameters. For example, microparticles produced at higher precipitator temperature had lower water content; while microparticles produced at higher mass flow ratio (i.e. higher solution flow rate) had higher water content, as shown in Table 2. The water content could be controlled, but normally was higher than 5% in the present study. Rise of N_2 flow rate or precipitator temperature might be adapted to further decrease the water content in the final product. It was obvious that the beginning of the first stage weight loss in TGA thermograms was earlier for O-chitosan microparticles compared with the commercial raw material. At the same time, the onset of the first endotherm in the DSC thermograms of O-chitosan microparticles shifted to lower temperatures. The earlier water loss implied weaker water–polymer interactions which were also observed while micronizing chitosan using SAA process (Reverchon & Antonacci, 2006).

The second stage of weight loss beginning at around 100 °C was due to the decomposition of O-chitosan molecules, which also caused an exotherm in DSC thermograms (Qin, Wang, Peng, Hu, & Li, 2008). According to the TGA derivative, the onset temperature of active pyrolysis (T_{onset}) remained unchanged for SAA-HCM produced O-chitosan microparticles compared with raw material. This could be confirmed in DSC thermograms since the onset of exothermic effect was at the same temperature for all samples. Moreover, the maximum pyrolysis happened at the same temperature (T_p) for all microparticle samples and the raw material. It is evident that the thermal stability of O-chitosan was substantially preserved during SAA-HCM processing.

3.3. Theoretical aerodynamic diameters

The powder densities were determined using a tapping method. It is notable that all powder samples analyzed had densities lower than 0.45 g/cm^3, which can be an indication of hollow or porous structure since the true density of saccharides lays around 1.6 g/cm^3. This is somehow useful for delivery systems like inhaled dry powders for a better deposition performance (Musante, Schroeter, Rosati, Crowder, Hickey, & Martonen, 2002). As can be seen in Table 2, the tap densities of the SAA-HCM produced microparticles increased with higher solution concentration, which was the result of the increased solid content in the droplet under the mechanism of “one droplet one particle” (runs 12, 3 and 14). The higher precipitator temperature resulted in lower powder density, accompanied with lower water content (run 4). This was reasonable because higher drying rate may cause unstable shell formation and subsequently extra hollow structure and deflated surfaces, as shown in Fig. 2(e), and the decreased water content led to lower density. In addition, the increase of density at higher mass flow ratio was also the result of changed water content (run 10).

The theoretical estimation of aerodynamic diameters could give reasonable anticipation for the potential dispersing and depositing performance of powders, which were normally determined by inertial impactors or aerosizer (Vanbever, Mintzes, Wang, Nice, Chen, Batycky, Langer, & Edwards, 1999). According to the definition of *MMADt*, the increase of density together with the increase of *VMD* caused larger *MMADt*, which is the case of increasing solution concentration in Table 2 (runs 12, 3 and 14). Except for powders produced at very low concentration (run 12),

Table 2
Size, density and water content for typical samples of O-chitosan microparticles.

Run no.	Mean diameter (μm)	*VMD* (μm)	Tap density (g/cm^3)	*MMADt* (μm)	Water content (%)
3	1.19 ± 0.071	1.87 ± 0.09	0.41 ± 0.007	1.20 ± 0.06	7.74 ± 0.17
4	1.23 ± 0.043	2.07 ± 0.13	0.38 ± 0.009	1.28 ± 0.08	6.42 ± 0.18
10	1.31 ± 0.082	2.30 ± 0.12	0.43 ± 0.010	1.52 ± 0.09	8.31 ± 0.25
12	0.85 ± 0.033	1.38 ± 0.05	0.37 ± 0.013	0.84 ± 0.04	5.75 ± 0.12
14	1.45 ± 0.067	2.61 ± 0.15	0.44 ± 0.014	1.74 ± 0.12	8.42 ± 0.29

all powder samples were calculated to have *MMADt* in the range of 1–2 μm. Thus, for SAA-HCM produced O-chitosan microparticles, the aerodynamic sizes centered in the respirable range, together with the very narrow size distributions characteristic, would render them potentially preferable for inhaled formulations, where O-chitosan can act as either the drug itself or an absorption enhancer.

4. Conclusions

The biopolymer of chitosan oligomers (O-chitosan) was successfully micronized into spherical micrometric particles with narrow size distributions using a novel SAA-HCM technique from aqueous solutions. Particle morphologies were mainly affected by precipitator temperature, while particle size tailoring was attainable by tuning other operation parameters. The structure and thermal stability of O-chitosan were well retained after SAA-HCM processing, but with lower crystallinity. Though highly hygroscopic, O-chitosan could be dried to an acceptable extent with water contents below 6% in this work. Modifications on N_2 flow rate or precipitator temperature will be helpful for further moisture content reduction. The aerodynamic sizes of microparticles were calculated to be inside 1–2 μm, which will be suitable for inhaled powder drug delivery systems. The successful micronization of O-chitosan expanded the application of SAA-HCM and implied the possibility of O-chitosan micropaticles as a drug/carrier. Moreover, the positive results on processability of O-chitosan brought the potential of SAA-HCM technique for producing O-chitosan based protein composite microparticles, where O-chitosan exerts its absorption enhancing ability.

Acknowledgements

The authors would thank gratefully for financial support provided by the National Natural Science Foundation of China and the Specialized Research Fund for the Doctoral Program of Higher Education of China (No. 20110101110032).

References

Adami, R., Liparoti, S., Izzo, L., Pappalardo, D., & Reverchon, E. (2012). PLA–PEG copolymers micronization by supercritical assisted atomization. *Journal of Supercritical Fluids*, *72*, 15–21.

Adami, R., Liparoti, S., & Reverchon, E. (2011). A new supercritical assisted atomization configuration for the micronization of thermolabile compounds. *Chemical Engineering Journal*, *173*, 55–61.

Adami, R., Osseo, L. S., & Reverchon, E. (2009). Micronization of lysozyme by supercritical assisted atomization. *Biotechnology and Bioengineering*, *104*, 1162–1170.

Adami, R., & Reverchon, E. (2012). Composite polymer-Fe_3O_4 microparticles for biomedical applications, produced by supercritical assisted atomization. *Powder Technology*, *218*, 102–108.

Amidi, M., Mastrobattista, E., Jiskoot, W., & Hennink, W. E. (2010). Chitosan-based delivery systems for protein therapeutics and antigens. *Advanced Drug Delivery Reviews*, *62*, 59–82.

Amidi, M., Pellikaan, H. C., de Boer, A. H., Crommelin, D. J. A., Hennink, W. E., & Jiskoot, W. (2008). Preparation and physicochemical characterization of supercritically dried insulin-loaded microparticles for pulmonary delivery. *European Journal of Pharmaceutics and Biopharmaceutics*, *68*, 191–200.

Bailey, M. M., Gorman, E. M., Munson, E. J., & Berkland, C. (2008). Pure insulin nanoparticle agglomerates for pulmonary delivery. *Langmuir*, *24*, 13614–13620.

Buttini, F., Colombo, P., Rossi, A., Sonvico, F., & Colombo, G. (2012). Particles and powders: Tools of innovation for non-invasive drug administration. *Journal of Controlled Release*, *161*, 693–702.

Cai, M. Q., Guan, Y. X., Yao, S. J., & Zhu, Z. Q. (2008). Supercritical fluid assisted atomization introduced by hydrodynamic cavitation mixer (SAA-HCM) for micronization of levofloxacin hydrochloride. *Journal of Supercritical Fluids*, *43*, 524–534.

Caputo, G., Adami, R., & Reverchon, E. (2010). Analysis of dissolved-gas atomization: Supercritical CO_2 dissolved in water. *Industrial and Engineering Chemistry Research*, *49*, 9454–9461.

Du, Z., Guan, Y. X., Yao, S. J., & Zhu, Z. Q. (2011). Supercritical fluid assisted atomization introduced by an enhanced mixer for micronization of lysozyme: Particle morphology, size and protein stability. *International Journal of Pharmaceutics*, *421*, 258–268.

Du, Z., Tang, C., Guan, Y. X., Yao, S. J., & Zhu, Z. Q. (2013). Bioactive insulin microparticles produced by supercritical fluid assisted atomization with an enhanced mixer. *International Journal of Pharmaceutics*, *454*, 174–182.

Kiechel, M. A., & Schauer, C. L. (2013). Non-covalent crosslinkers for electrospun chitosan fibers. *Carbohydrate Polymers*, *95*, 123–133.

Kim, J. Y., Lee, J. K., Lee, T. S., & Park, W. H. (2003). Synthesis of chitooligosaccharide derivative with quaternary ammonium group and its antimicrobial activity against *Streptococcus mutans*. *International Journal of Biological Macromolecules*, *32*, 23–27.

Kittur, F. S., Prashanth, K. V. H., Sankar, K. U., & Tharanathan, R. N. (2002). Characterization of chitin, chitosan and their carboxymethyl derivatives by differential scanning calorimetry. *Carbohydrate Polymers*, *49*, 185–193.

Knez, Ž., Markočič, E., Novak, Z., & Hrnčič, M. K. (2011). Processing polymeric biomaterials using supercritical CO_2. *Chemie Ingenieur Technik*, *83*, 1371–1380.

Kumar, S., & Koh, J. (2013). Synthesis, physiochemical and optical properties of chitosan based dye containing naphthalimide group. *Carbohydrate Polymers*, *94*, 221–228.

Liparoti, S., Adami, R., & Reverchon, E. (2012). PEG micronization by supercritical assisted atomization, operated under reduced pressure. *Journal of Supercritical Fluids*, *72*, 46–51.

Miao, S. F., Yu, J. P., Du, Z., Guan, Y. X., Yao, S. J., & Zhu, Z. Q. (2010). Supercritical fluid extraction and micronization of ginkgo flavonoids from *Ginkgo biloba* leaves. *Industrial and Engineering Chemistry Research*, *49*, 5461–5466.

Musante, C. J., Schroeter, J. D., Rosati, J. A., Crowder, T. M., Hickey, A. J., & Martonen, T. B. (2002). Factors affecting the deposition of inhaled porous drug particles. *Journal of Pharmaceutical Sciences*, *91*, 1590–1600.

Muzzarelli, R. A. A. (2009). Chitins and chitosans for the repair of wounded skin, nerve, cartilage and bone. *Carbohydrate Polymers*, *76*, 167–182.

Muzzarelli, R. A. A. (2010). Enhanced biochemical efficacy of oligomeric and partially depolymerized chitosans. In F. Columbus (Ed.), *Chitosan: Manufacture, properties and usages*. Hauppauge, NY, USA: Nova Publishing.

Muzzarelli, R. A. A., Stanic, V., & Ramos, V. (1999). Enzymatic depolymerization of chitins and chitosans. In C. Bucke (Ed.), *Methods in biotechnology: Carbohydrate biotechnology protocols*. Totowa: Humana Press.

Prasertsung, I., Damrongsakkul, S., Terashima, C., Saito, N., & Takai, O. (2012). Preparation of low molecular weight chitosan using solution plasma system. *Carbohydrate Polymers*, *87*, 2745–2749.

Qin, C. Q., Wang, W., Peng, H. E., Hu, R., & Li, W. (2008). Preparation and properties of reduced chitooligomers. *Carbohydrate Polymers*, *72*, 701–706.

Reverchon, E. (2002). Supercritical-assisted atomization to produce micro- and/or nanoparticles of controlled size and distribution. *Industrial and Engineering Chemistry Research*, *41*, 2405–2411.

Reverchon, E., & Adami, R. (2013). Supercritical assisted atomization to produce nanostructured chitosan–hydroxyapatite microparticles for biomedical application. *Powder Technology*, *246*, 441–447.

Reverchon, E., & Antonacci, A. (2006). Chitosan microparticles production by supercritical fluid processing. *Industrial and Engineering Chemistry Research*, *45*, 5722–5728.

Reverchon, E., & Antonacci, A. (2007a). Drug–polymer microparticles produced by supercritical assisted atomization. *Biotechnology and Bioengineering*, *97*, 1626–1637.

Reverchon, E., & Antonacci, A. (2007b). Polymer microparticles production by supercritical assisted atomization. *Journal of Supercritical Fluids*, *39*, 444–452.

Vanbever, R., Mintzes, J. D., Wang, J., Nice, J., Chen, D. H., Batycky, R., Langer, R., & Edwards, D. A. (1999). Formulation and physical characterization of large porous particles for inhalation. *Pharmaceutical Research*, *16*, 1735–1742.

Wang, Q., Guan, Y. X., Yao, S. J., & Zhu, Z. Q. (2010). Microparticle formation of sodium cellulose sulfate using supercritical fluid assisted atomization introduced by hydrodynamic cavitation mixer. *Chemical Engineering Journal*, *159*, 220–229.

Wang, Q., Guan, Y. X., Yao, S. J., & Zhu, Z. Q. (2011). Controllable preparation and formation mechanism of BSA microparticles using supercritical assisted atomization with an enhanced mixer. *Journal of Supercritical Fluids*, *56*, 97–104.

Wiebe, R. (1941). The binary system carbon dioxide–water under pressure. *Chemical Reviews*, *29*, 475–481.

Zeng, L. T., Qin, C. Q., Chi, W. L., Wang, L. S., Ku, Z. J., & Li, W. (2007). Browning of chitooligomers and their optimum preservation. *Carbohydrate Polymers*, *67*, 551–558.